Electronic Supplementary Material (ESI) for CrystEngComm.

SUPPORTING INFORMATION

Doubly interpenetrated indium-tricarboxylate frameworks mediated by small molecules with enhanced porosity

Yujing Du[a], Li Zhong[a], Yue Hu[a], Qipeng Li*[b], and Jinjie Qian*[a]

[a]*College of Chemistry and Materials Engineering, Wenzhou University, Wenzhou 325035, P. R. China.*

[b]*College of Chemistry and Chemical Engineering, Zhaotong University, Zhaotong 657000, P. R. China.*

**To whom correspondence should be addressed: E-mail: jinjieqian@wzu.edu.cn; E-mail: liqipeng10@mails.ucas.ac.cn.*

Table of Content

S1. Materials and Methods

1.1. Materials and Instruments

All the reactants are of reagent-grade quality and used as purchased commercially without further purification. The power X-ray diffraction patterns (PXRD) were collected by a Bruker D8 Advance using Cu Kα radiation (λ = 0.154 nm). Thermogravimetric analyses were recorded on a NETZSCH STA 449C unit at a heating rate of 10 $^{o}C\cdot min^{-1}$ under flowing nitrogen atmosphere. Elemental analyses were measured with an Elemental Vairo Micro Analyzer. Single gas adsorption measurements were performed in the Accelerated Surface Area and Porosimetry 2020 (ASAP 2020).

1.2. Synthesis Procedures

Reactions were carried out in 20 ml glass vials under autogenous pressure. All the reactants are of reagent-grade quality and used as commercially purchased without further purification.

Synthesis of $[In(BTB)(NMF)_2]\bullet H_2O$ (InOF-19)

The solvothermal reaction of a mixture of $In(NO_3)_3\cdot 6H_2O$ (0.10 mmol, 33 mg) and H_3BTB (0.05 mmol, 20 mg, H_3BTB = 1,3,5-tris(4-carboxyphenyl)benzene) in N-methylformamide (NMF) (3 mL) and MeCN (3 mL) with an additional 0.1 ml HNO_3 (65 wt %) was taking place in a 20 mL glass vial, which was transferred into an oven holding at 85 ^{o}C for 5 days. After being centrifugated and washed by fresh ethanol for 3 times, the crystals of solvated **InOF-19** were successfully obtained in *ca*. 46% yield based on indium salt. Elemental analysis was calculated for **InOF-19**: C, 54.25%; H, 3.97%; N, 4.08%. Found: C, 54.32%; H, 4.04%; N, 3.98%. The phase purity of the sample was also confirmed by PXRD (Figure S10).

Synthesis of $[In(BTB)(DMA)]\bullet H_2O$ (InOF-20)

Similarly, the solvothermal reaction of a mixture of $In(NO_3)_3$ (0.10 mmol, 33mg) and H_3BTB (0.05 mmol, 20 mg) in N,N-Dimethylacetamide (DMA) (5 mL) with an additional 0.1 ml HNO_3 takes place in a vial at 85 ^{o}C for 5 days. After being centrifugated and washed by fresh ethanol for 3 times, the crystals of solvated **InOF-20** were successfully obtained in *ca*. 58% yield based on indium salt. Elemental analysis was calculated for **InOF-20**: C, 56.81%; H, 3.99%; N, 2.14%. Found:

C, 56.86%; H, 3.95%; N, 2.13%. The phase purity of the sample was also confirmed by PXRD (Figure S11).

Synthesis of $(Et_2NH_2)_2[In_2(BTB)_2(INC)_2]$•DEF•$3H_2O$ (InOF-21)

Similarly, the solvothermal reaction of a mixture of $In(NO_3)_3$ (0.10 mmol, 33mg), H_3BTB (0.05 mmol, 20 mg), HINC (0.05mmol, 6 mg, HINC = Isonicotinic acid) in N,N-Diethylformamide (DEF) (5 mL) with an additional 0.1 ml HNO_3 takes place in a vial at 85 ^oC for 5 days. After being centrifugated and washed by fresh ethanol for 3 times, the crystals of solvated **InOF-21** were successfully obtained in *ca*. 51% yield based on indium salt. Elemental analysis was calculated for **InOF-21**: C, 57.57%; H, 4.83%; N, 4.25%. Found: C, 57.962%; H, 4.77%; N, 4.29%. The phase purity of the sample was also confirmed by PXRD (Figure S12).

Synthesis of $(Et_2NH_2)_2[In_2(BTB)_2(OX)]$•$6H_2O$ (InOF-22)

Similarly, the solvothermal reaction of a mixture of $In(NO_3)_3$ (0.10 mmol, 33mg), H_3BTB (0.05 mmol, 20 mg), H_2OX (0.05mmol, 4.5 mg, H_2OX = Oxalic acid) in N,N-Diethylformamide (DEF) (5 mL) with an additional 0.1 ml HNO_3 takes place in a vial at 85 ^oC for 5 days. After being centrifugated and washed by fresh ethanol for 3 times, the crystals of solvated **InOF-22** were successfully obtained in *ca*. 42% yield based on indium salt. Elemental analysis are tested for as-made materials **InOF-22**: Calculated:C, 53.20%; H, 4.60%; N, 1.94%. Found: C, 50.91%; H, 4.98%; N, 1.34%. The phase purity of the sample was also confirmed by PXRD (Figure S13). In this case, we learn that the charge of the whole framework in **InOF-22** is negative. Therefore, we assume that there must be disordered $Et_2NH_2^+$counter-cations randomly lying inside the large solvent accessible void, which are the byproduct of in situ decomposition of the N, N'-diethylformamide solvent, thus leading to the final charge equilibrium.

1.3. Single-Crystal X-ray Crystallography

The structure data of **InOF-19, InOF-20, InOF-21** and **InOF-22**were collected on a SuperNova, Dual, *Cu* at zero, Atlasdiffractometer. The crystals were kept at 99.99(16) K during data collection. Using Olex2,[S1] the structure was solved with the ShelXS[S2] structure solution

program using Direct Methods and refined with the ShelXL[S3] refinement package using Least Squares minimisation. Crystallographic data and structure refinement parameters for these four crystals are listed in Table S1. We employed PLATON/SQUEEZE[S4] to calculate the contribution to the diffraction from the solvent region and there by produced a set of solvent-free diffraction intensities. The final formulae were calculated from the SQUEEZE results combined with elemental analysis data and TGA data. More details on the crystallographic studies as well as atomic displacement parameters are given in Supporting Information as CIF files. Crystallographic data for the structure reported in this paper has been deposited. The following crystal structure has been deposited at the Cambridge Crystallographic Data Centre and allocated the deposition number (CCDC No.) 1886112, 1886113, 1886114 and1886115 for **InOF-20**, **InOF19**, **InOF-22** and **InOF-21**, respectively.These data can be obtained free of charge via *www.ccdc.cam.ac.uk/data_request/ cif.*

Table S1 Summary of Crystal Data and Refinement Parameters of **InOF-19~22**.

Items	**InOF-19**	**InOF-20**	**InOF-21**	**InOF-22**
CCDC	1886113	1886112	1886115	1886114
formula	$C_{31}H_{25}N_2O_8In_1$	$C_{31}H_{24}N_1O_7In_1$	$C_{66}H_{38}N_2O_{16}In_2$	$C_{28}H_{15}O_8In_1$
Mass	668.35	637.33	1344.62	594.22
crystal system	Monoclinic	Orthorhombic	Triclinic	Monoclinic
space group	$P2_1/n$	*P*bcn	*P*-1	*I*2/m
a (Å)	8.57760(10)	17.4900(3)	9.0282(2)	17.5673(3)
b (Å)	26.9064(5)	21.7156(3)	15.3282(3)	25.7031(5)
c (Å)	15.5158(2)	16.5786(3)	26.6329(5)	24.4991(4)
α (°)	90.00	90.00	90.906(2)	90.00
β(°)	91.2330(10)	90.00	91.479(2)	91.1550(10)
γ(°)	90.00	90.00	98.927(2)	90.00

V (Å^3)	3580.10(9)	6296.65(18)	3639.03(13)	11059.9(3)
T (K)	296(2)	296(2)	296(2)	296(2)
Z	4	8	2	8
F(000)	1352	2576	1348	2368
GOF	1.076	1.097	1.181	1.006
R_1 (I>2σ(I))	0.0346	0.0604	0.0907	0.0641
wR_2 (all reflections)	0.1007	0.1744	0.2171	0.1810

S2. Additional X-ray Crystal Structural Figures

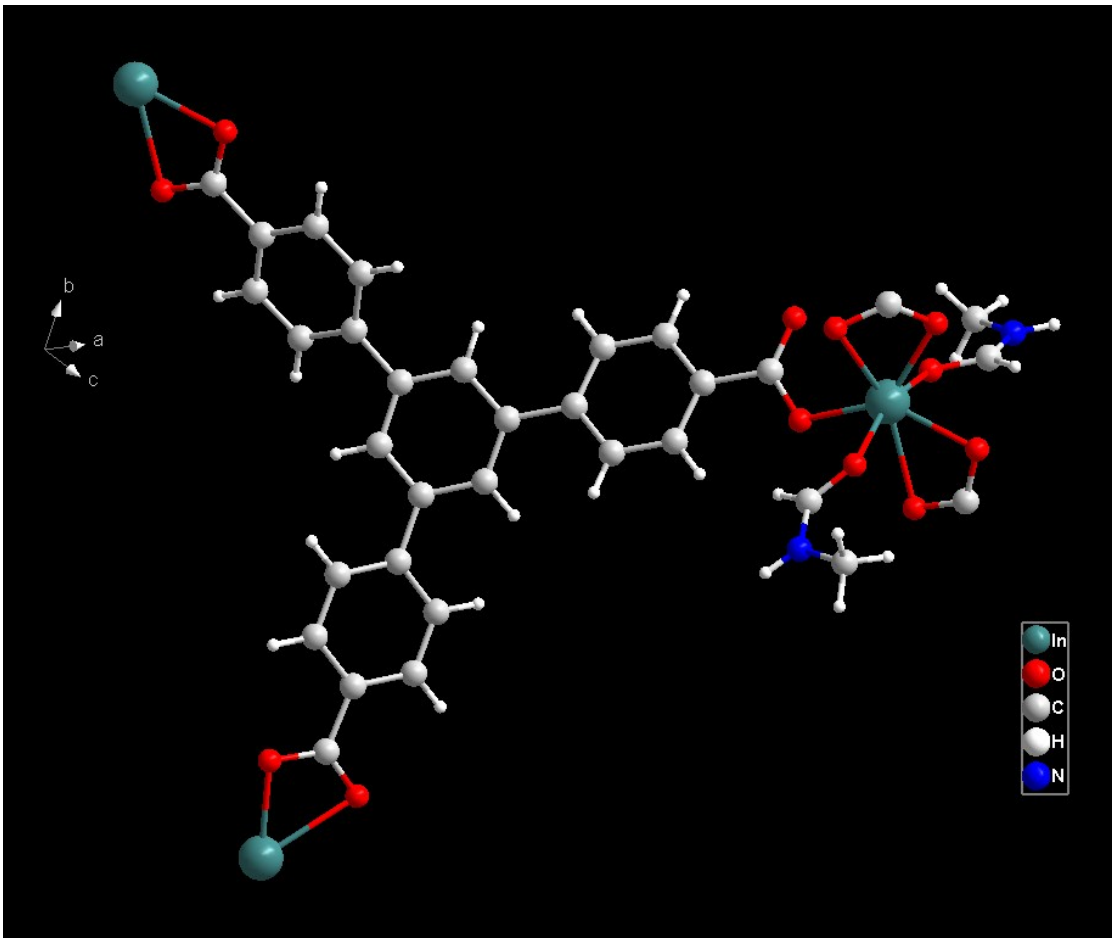

Figure S1. The asymmetric unit and the coordination environment of the central In(III) atoms in **InOF-19**.

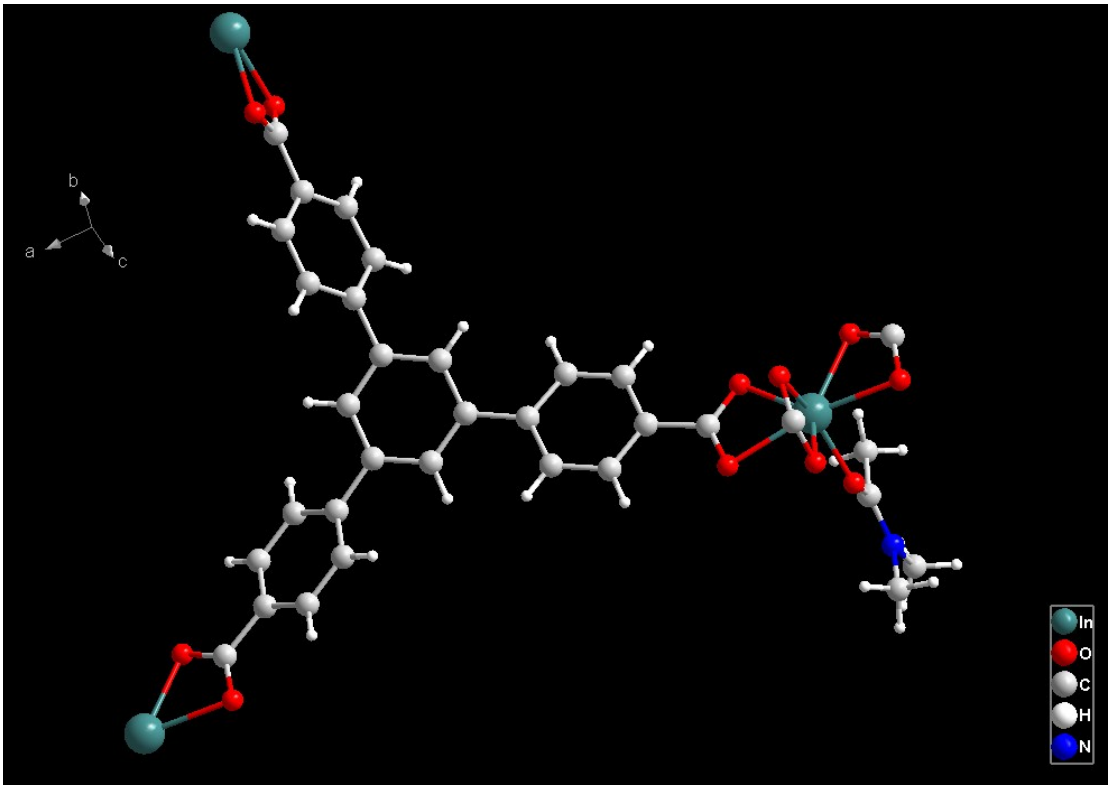

Figure S2. The asymmetric unit and the coordination environment of the central In(III) atoms in **InOF-20**.

InOF-20 (In-BTB-DMA) crystallizes in the orthorhombic space group *P*bcn and its asymmetric unit contains one In(III) ion, one BTB^{3-} ligand and one coordinated DMA molecule. The In(III) centre is seven-coordinated by six carboxylate oxygen atoms from three separate BTB^{3-} ligands and one oxygen atoms from one DMA molecule, to form the $[InO(CO_2)_3]$ moiety (Figure S2 and Figure S5).

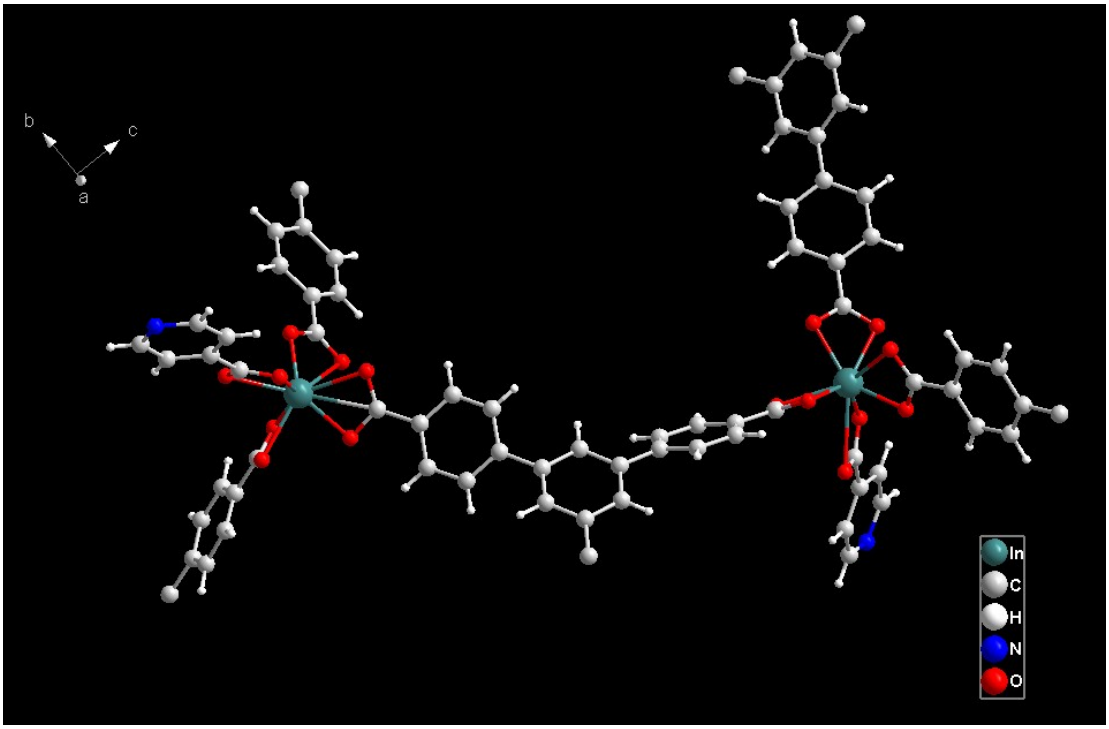

Figure S3. The asymmetric unit and the coordination environment of the central In(III) atoms in **InOF-21**.

InOF-21 (In-BTB-INC) crystallizes in the triclinic space group *P*-1 with the asymmetric unit including two In(III) ions, two BTB^{3-} ligands and INC^{-} ligand. Structurally speaking, each In(III) ion is 8-coordinated to six carboxylate oxygen atoms from three separate BTB^{3-} ligands and another two carboxylate oxygen atoms from one INC^{-} ligand, to constitute a $[In(CO_2)_4]$ moiety (Figure S3 and Figure S5).

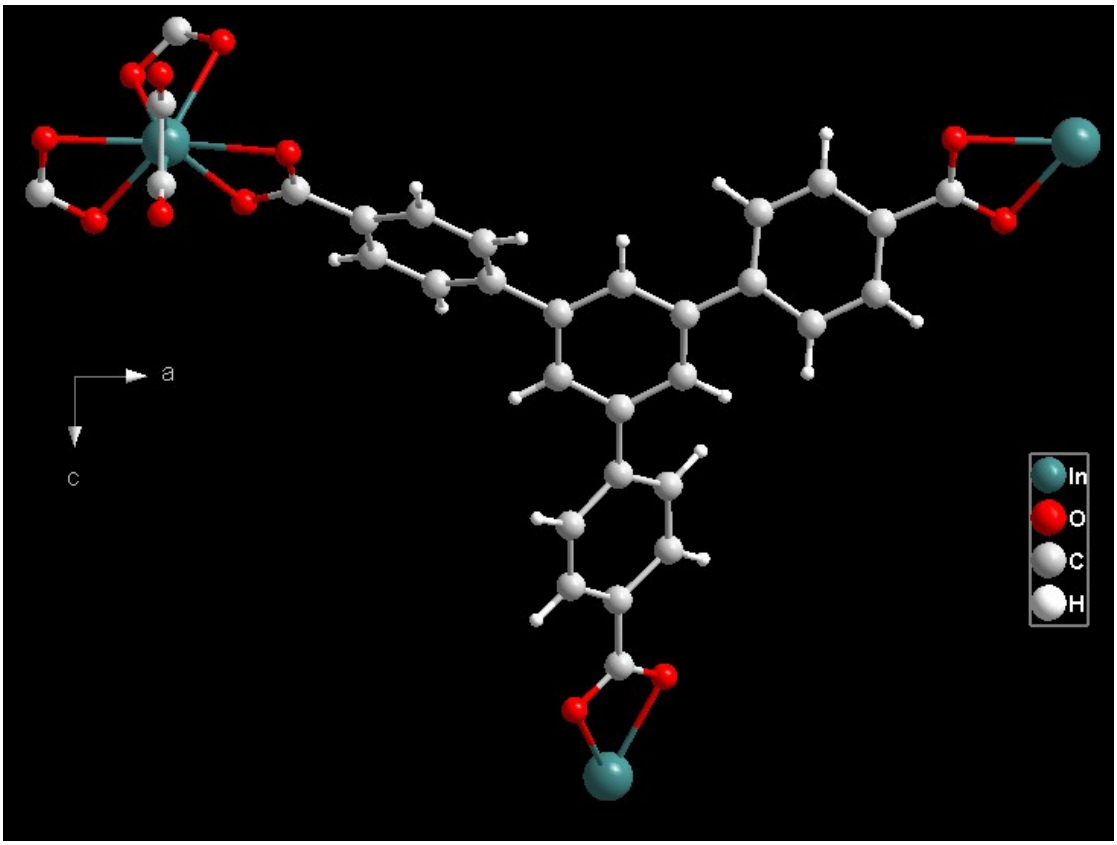

Figure S4. The asymmetric unit and the coordination environment of the central In(III) atoms in **InOF-22**.

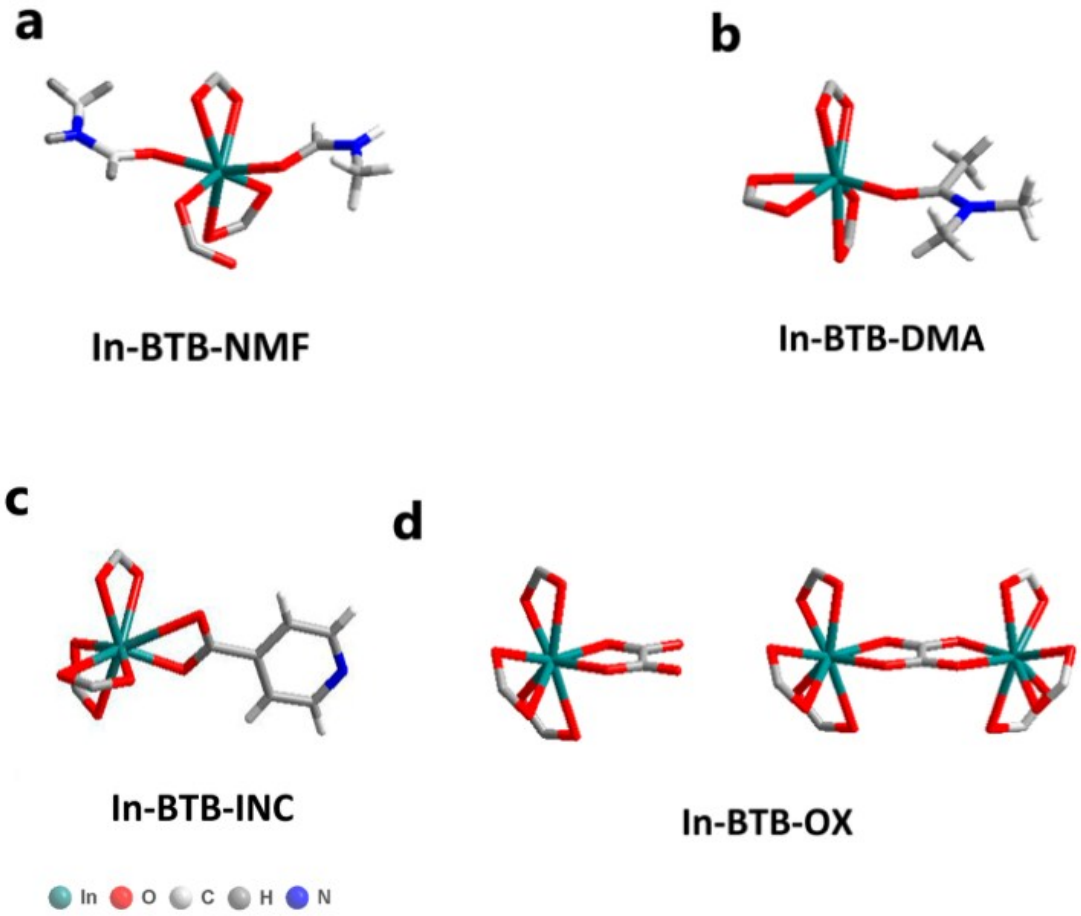

Figure S5. All structures are built upon a typical 8-coordinated $[In(COO)_4]^-$ secondary building blocks, in which one of carboxylate groups are replaced by **(a)** two NMFs in **InOF-19**; **(b)** one DMA in **InOF-20**; **(c)** one deprotonated HINC in **InOF-21**; and **(d)** one fully deprotonated H_2OX molecules in **InOF-22**, and the right-handed end also presents a dinuclear In-based SBU by a bridging OX^{2-} linker.

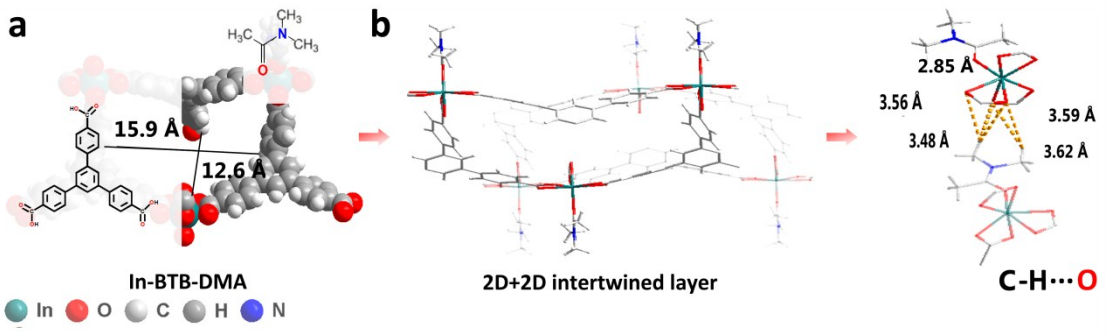

Figure S6. The window and 2D + 2D interpenetrated layer in In-BTB-DMA. **(a)** H_3BTB ligand, DMA molecule and the window in a 2D layer representative of **InOF-20** (In-BTB-DMA). **(b)** 2D + 2D interpenetrated layer with the phenyl C-H···O hydrogen bond interaction .

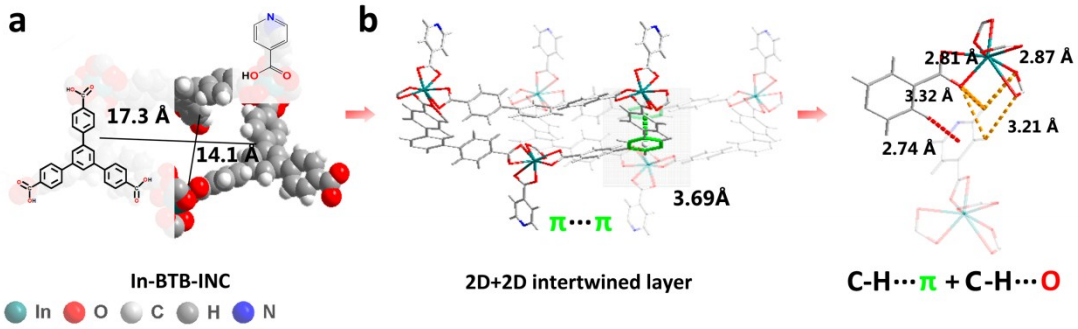

Figure S7. The window and 2D + 2D interpenetrated layer within the π-π stacking as well as C-H···πhydrogen bond interaction in In-BTB-INC. **(a)** H_3BTB ligand, HINC molecule and the window in a 2D layer representative of **InOF-21** (In-BTB-INC).**(b)** 2D + 2D interpenetrated layer with the phenyl C-H···O hydrogen bond interaction as well the phenyl C-H···πhydrogen bond interaction.

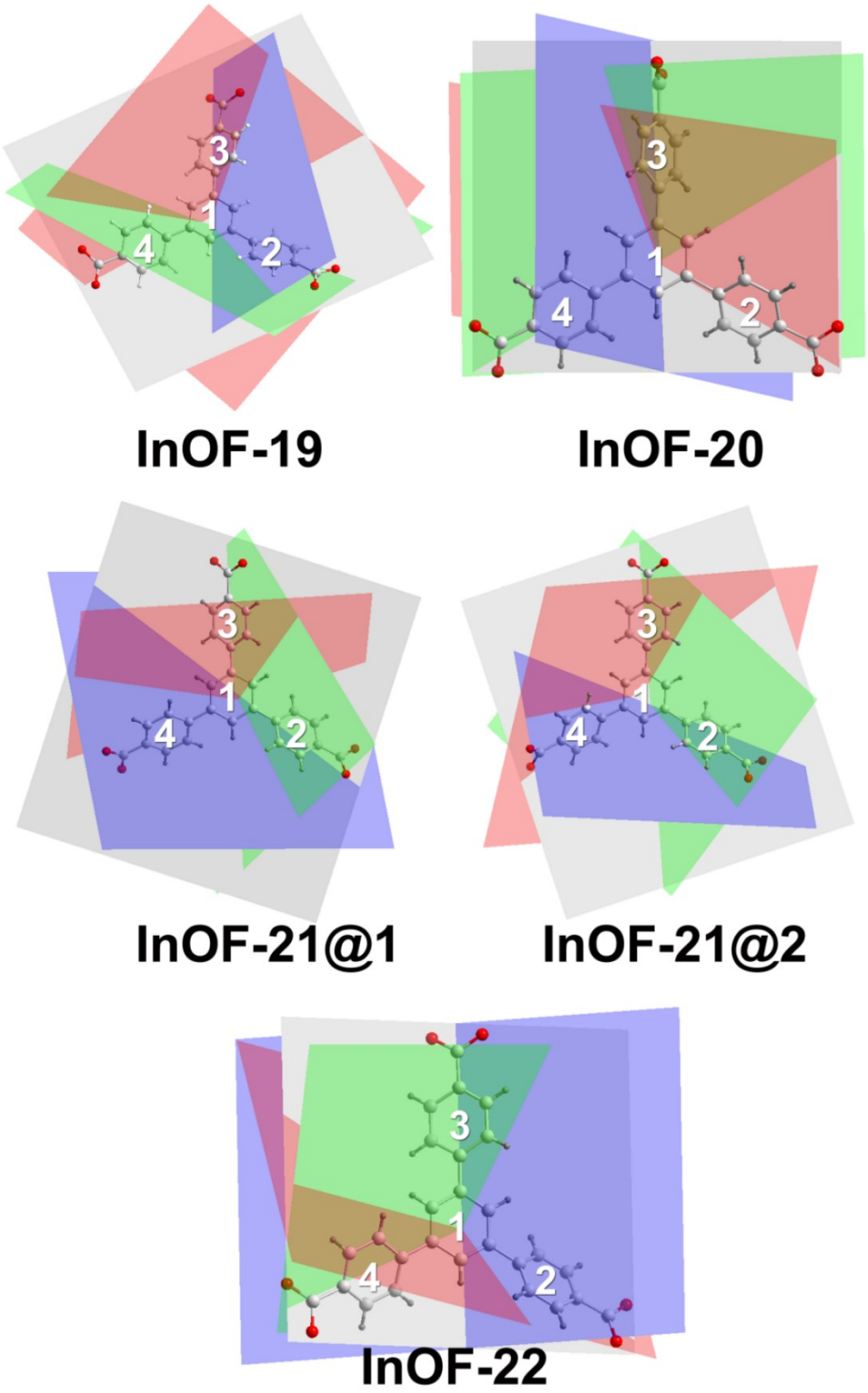

Figure S8. Dihedral angles between these phenyl rings in tricarboxylate BTB(III) ligands in **InOF-19~22**.

Note that there are two crystallographically different phenyl rings in **InOF-21**.

Table S2. Summary of the dihedral angles between these phenyl rings in tricarboxylate BTB(III) ligands in **InOF-19~22.**

	InOF-19	**InOF-20**	**InOF-21**		**InOF-22**
Plane 1 and Plane 2 (°)	33.039(84)	56.595(12)	38.072(22)	41.094(23)	37.085(14)
Plane 1 and Plane 3 (°)	32.619(84)	38.308(13)	38.068(21)	35.074(21)	35.125(12)
Plane 1 and Plane 4 (°)	18.422(74)	20.805(12)	37.713(23)	31.949(24)	25.143(16)

S3. Topological Analysis

Topology for2-dimensional interpenetrated layers for **InOF-19~21**

In(III) links by bridge ligands and has

Common vertex with					R(A-A)	
Ti 1	0.2387	1.1168	-0.0479	(0 1-1)	9.467A	1
Ti 1	1.2387	1.1168	0.9521	(1 1 0)	9.974A	1
Ti 1	0.2613	0.6168	0.5479	(0 0 1)	10.016A	1

Topology for Ti1

BTB^{3-} links by bridge ligands and has

Common vertex with					R(A-A)	
In(III)	0.6380	-0.0347	1.4613	(0-1 1)	9.467A	1
In(III)	-0.3620	-0.0347	0.4613	(-1-1 0)	9.974A	1
In(III)	-0.1380	0.4653	1.0387	(0-1 1)	10.016A	1

Structural group analysis

Structural group No 1

Structure consists of layers (1 0-1) with TiSc

Coordination sequences

In(III):	1	2	3	4	5	6	7	8	9	10
Num	3	6	9	12	15	18	21	24	27	30
Cum	4	10	19	31	46	64	85	109	136	166
BTB^{3-}:	1	2	3	4	5	6	7	8	9	10
Num	3	6	9	12	15	18	21	24	27	30
Cum	4	10	19	31	46	64	85	109	136	166

TD10=166

Vertex symbols for selected sublattice

In(III) Point (Schlafli) symbol:{6^3}

Extended point symbol:[6.6.6]

BTB^{3-} Point (Schlafli) symbol:{6^3}

Extended point symbol:[6.6.6]

Point (Schlafli) symbol for net: {6^3}

3-c net; uninodal net

Topological type: ***hcb***; Shubnikov hexagonal plane net/(6,3) (topos & RCSR.ttd) {6^3} - VS [6.6.6] (71251 types in 10 databases)

Topology for3-dimensional doubly interpenetrated framework for **InOF-22**

In(III)links by bridge ligands and has Common vertex with R(A-A)

BTB^{3-}	0.7482	0.1144	0.6253	(0 0 0)	9.695A	1
BTB^{3-}	0.2482	0.3856	0.1253	(0 0 0)	9.809A	1
BTB^{3-}	1.2482	0.3856	0.1253	(1 0 0)	9.851A	1

BTB^{3-}links by bridge ligands and has Common vertex with R(A-A)

BTB^{3-}	0.2482	0.6144	0.1253	(0 1 0)	5.880A	1
In(III)	0.2514	0.1896	-0.2128	(-1 0-1)	9.695A	1
In(III)	0.7514	0.3104	0.2872	(0 0 0)	9.809A	1
In(III)	-0.2486	0.3104	0.2872	(-1 0 0)	9.851A	1

Structure consists of 3D framework with TiSc

Coordination sequences

In(III): 1 2 3 4 5 6 7 8 9 10

Num 3 9 17 31 53 72 93 129 165 189

Cum 4 13 30 61 114 186 279 408 573 762

BTB^{3-}: 1 2 3 4 5 6 7 8 9 10

Num 4 9 19 35 50 70 102 127 155 205

Cum 5 14 33 68 118 188 290 417 572 777

TD10=769

Vertex symbols for selected sublattice

In(III) Point (Schlafli) symbol:{6^3}

Extended point symbol:[6.6.6(2)]

BTB^{3-} Point (Schlafli) symbol:{6^5.8}

Extended point symbol:[6.6.6.6.6.8(2)]

Point (Schlafli) symbol for net: **{6^3}{6^5.8}**

3,4-c net with stoichiometry (3-c)(4-c); 2-nodal net

Topological type:***fsc***-3,4-Imm2 (binodal.ttd) {6^3}{6^5.8} - VS [6.6.6.6.6.10(6)] [6.6.6(2)] (71251 types in 10 databases)

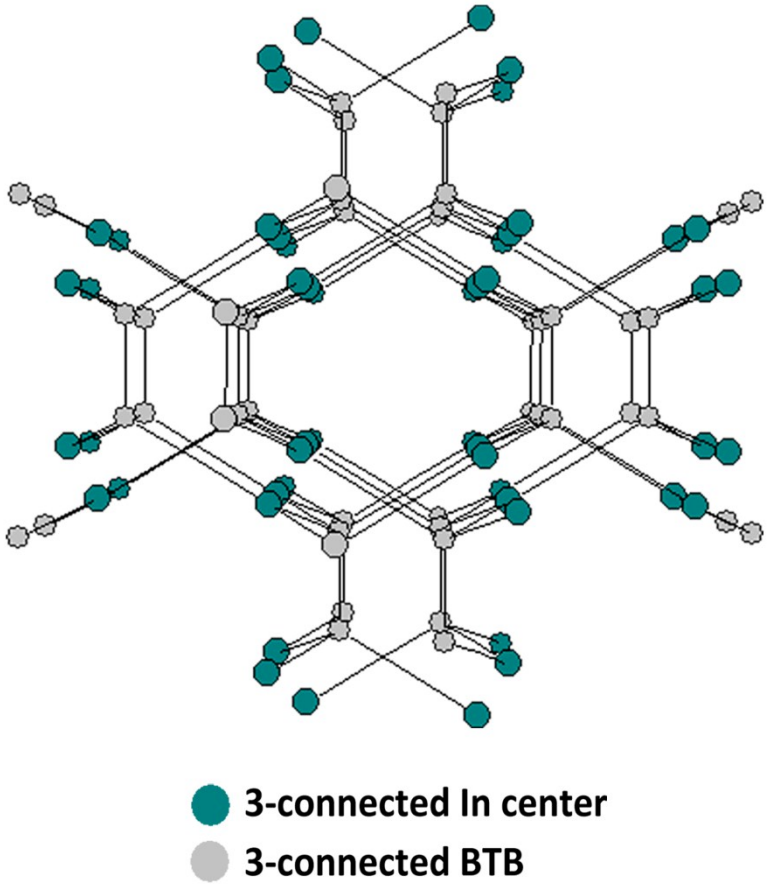

Figure S9. The 3-dimensional ***fsc*** networkof **InOF-22.**

S4. PXRD Data

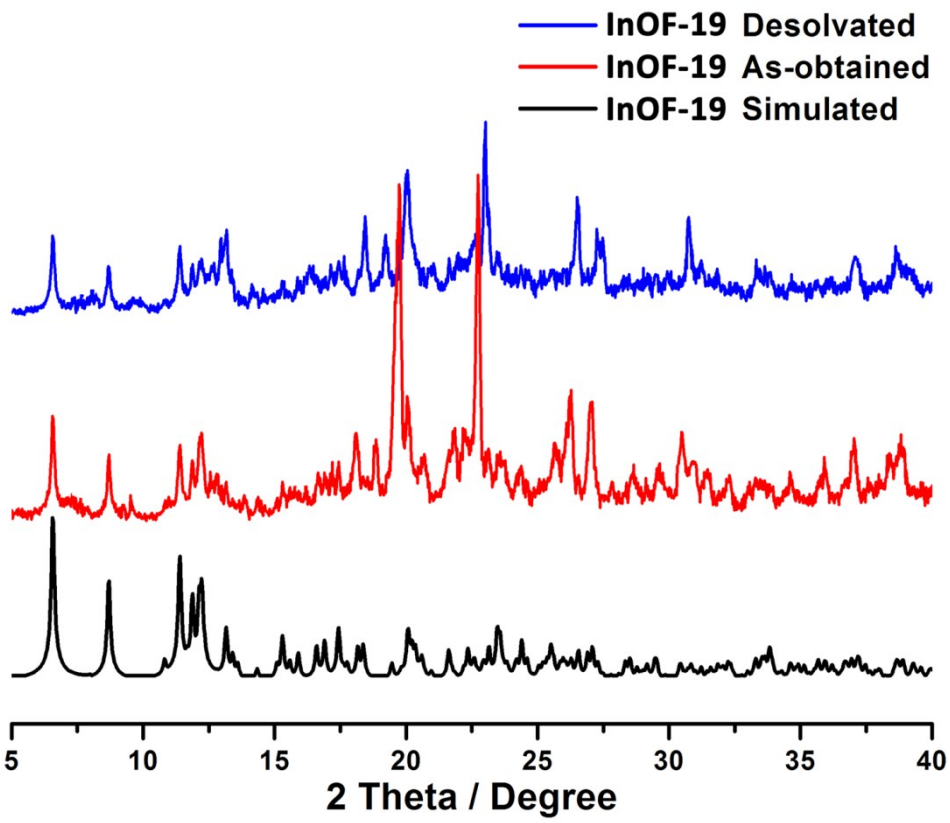

Figure S10. PXRD patterns of **InOF-19**: simulated from the crystallographic information file (black, bottom); from the as-prepared sample (red); from the desolvated sample (blue, top).

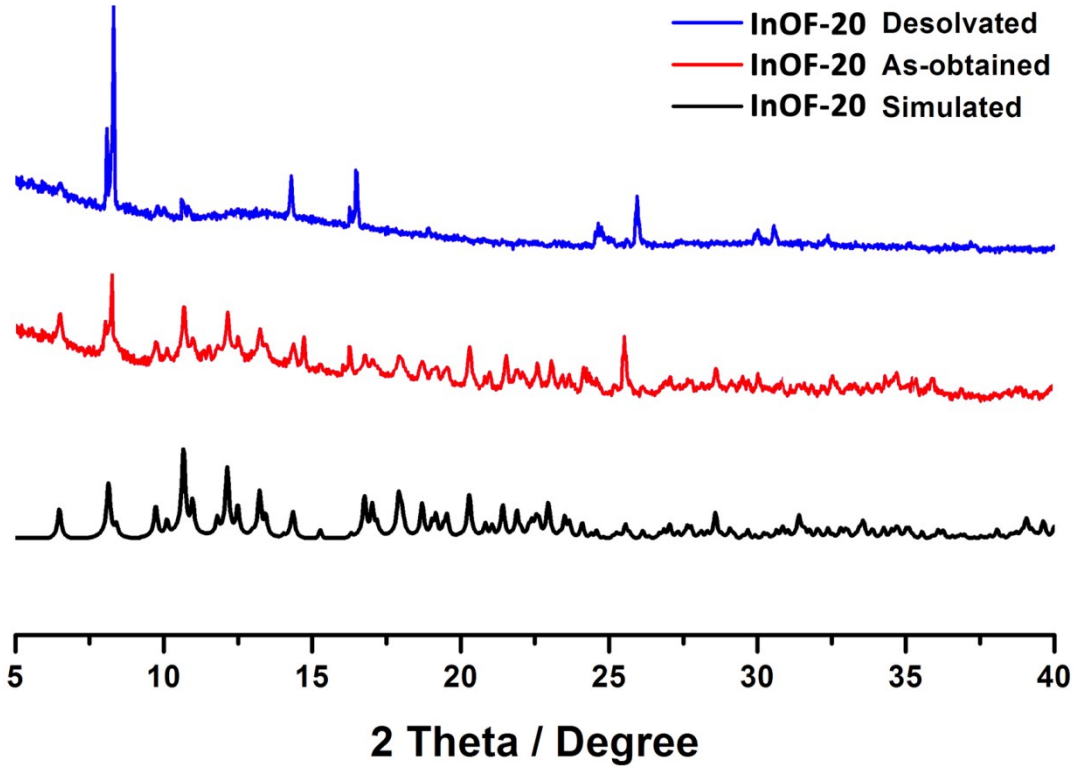

Figure S11. PXRD patterns of **InOF-20**: simulated from the crystallographic information file (black, bottom); from the as-prepared sample (red); from the desolvated sample (blue, top).

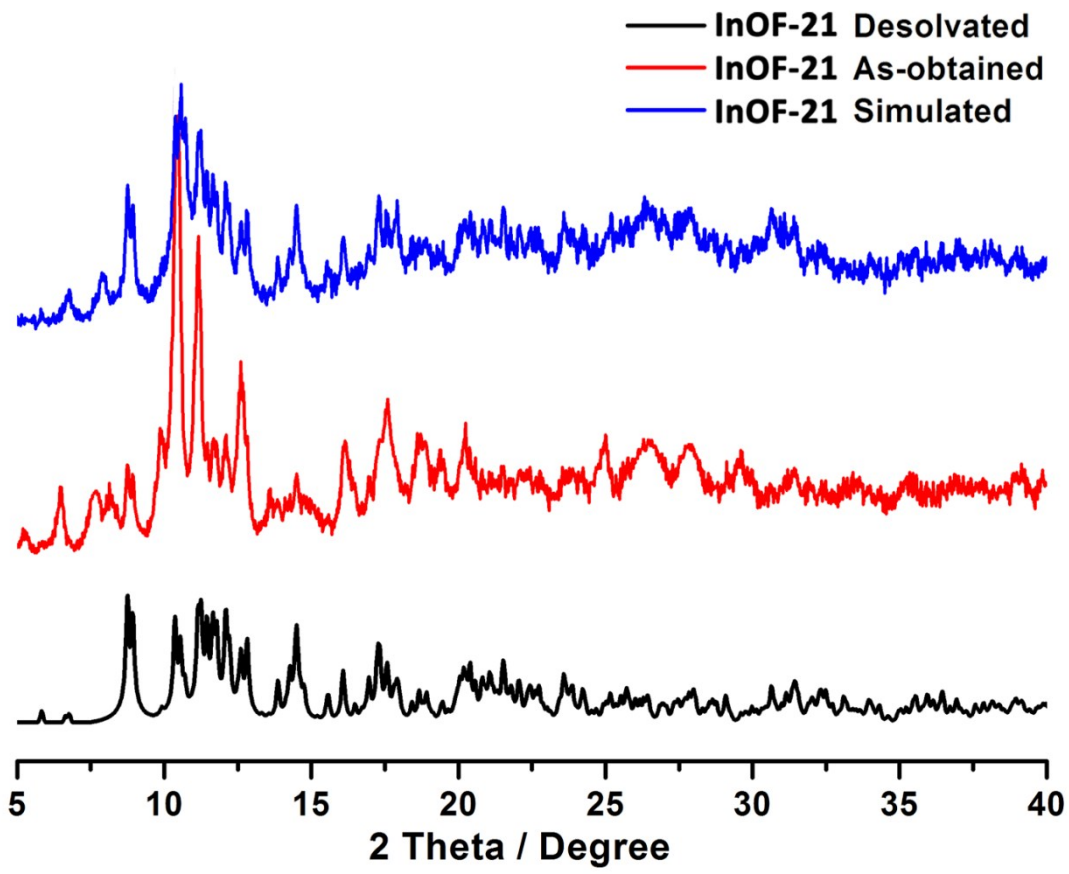

Figure S12. PXRD patterns of **InOF-21**: simulated from the crystallographic information file (black, bottom); from the as-prepared sample (red); from the desolvated sample (blue, top).

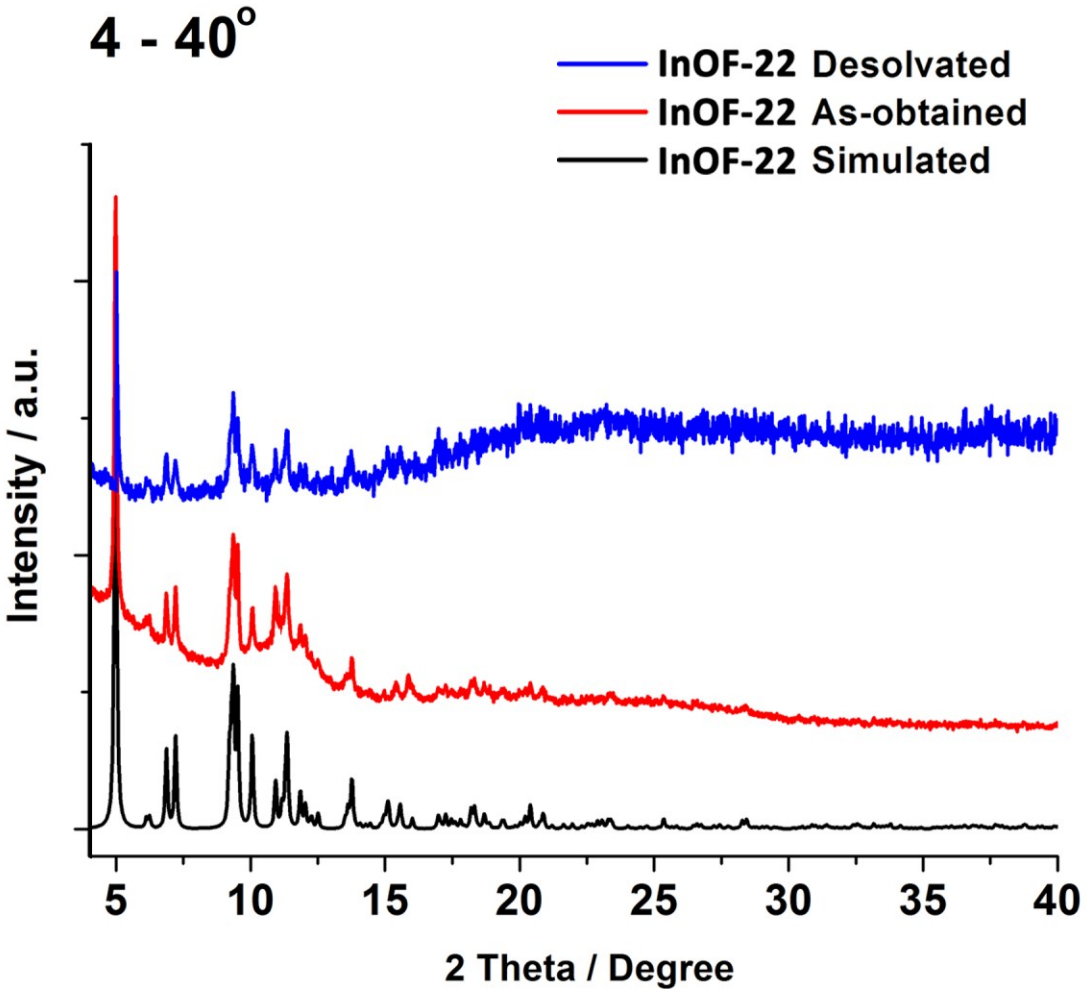

Figure S13. PXRD patterns of **InOF-22**: simulated from the crystallographic information file (black, bottom); from the as-prepared sample (red); from the desolvated sample (blue, top).

S5. TGA data and Analysis

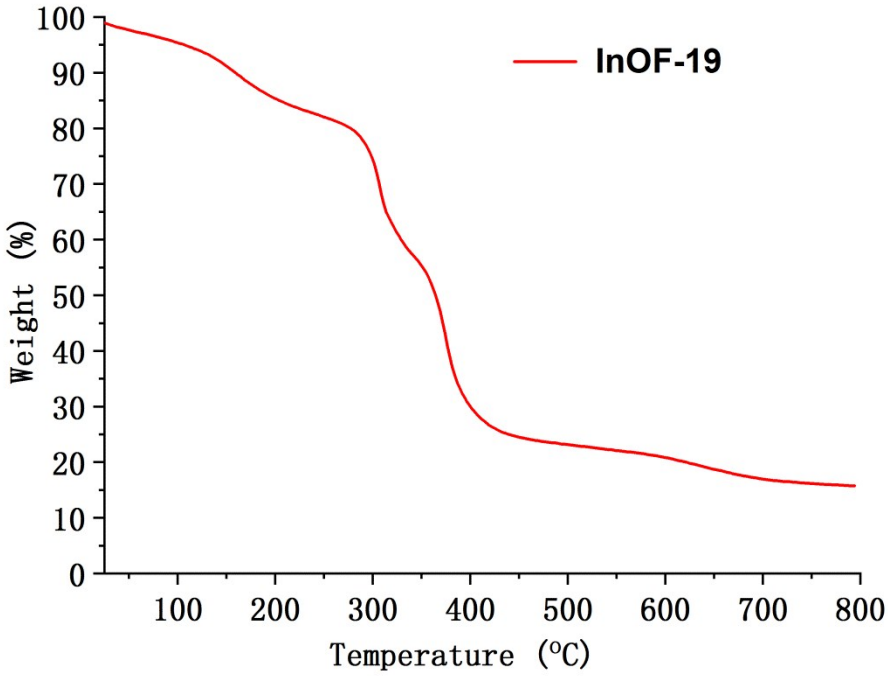

Figure S14. TGA curve for **InOF-19** samples.

Thermogravimetric analysis (TGA) measurements of **InOF-19** is conducted in the temperature range of 30-800 °C under a flow of nitrogen with the heating rate of 10°C min^{-1}. **InOF-19** shows a weight loss of ca.23.56% from 25-200 °C, which can be reasonably attributed to the loss of two coordinated NMF molecules and one guest H_2O molecule (calcd 23.92%), and then the main framework begins to quickly collapses upon further heating @ 400 °C (Figure S13).

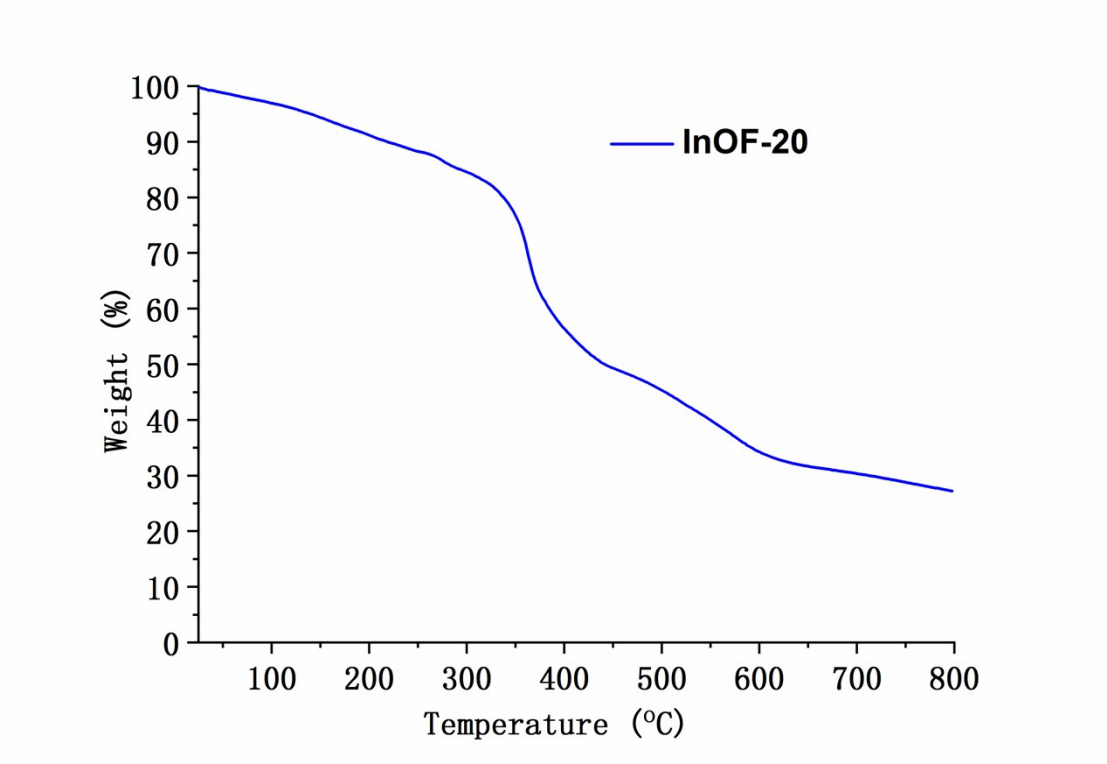

Figure S15. TGA curve for **InOF-20** samples.

Thermogravimetric analysis (TGA) measurements of **InOF-20** is conducted in the temperature range of 30-800 °C under a flow of nitrogen with the heating rate of 10°C min^{-1}.**InOF-20** shows a weight loss of ca.15.46% from 30-310 °C, which can be reasonably attributed to the loss of one coordinated DMA molecule and one guest H_2O molecule (calcd 16.04%), and then the main framework begins to quickly collapses upon further heating @ 350 °C (Figure S14).

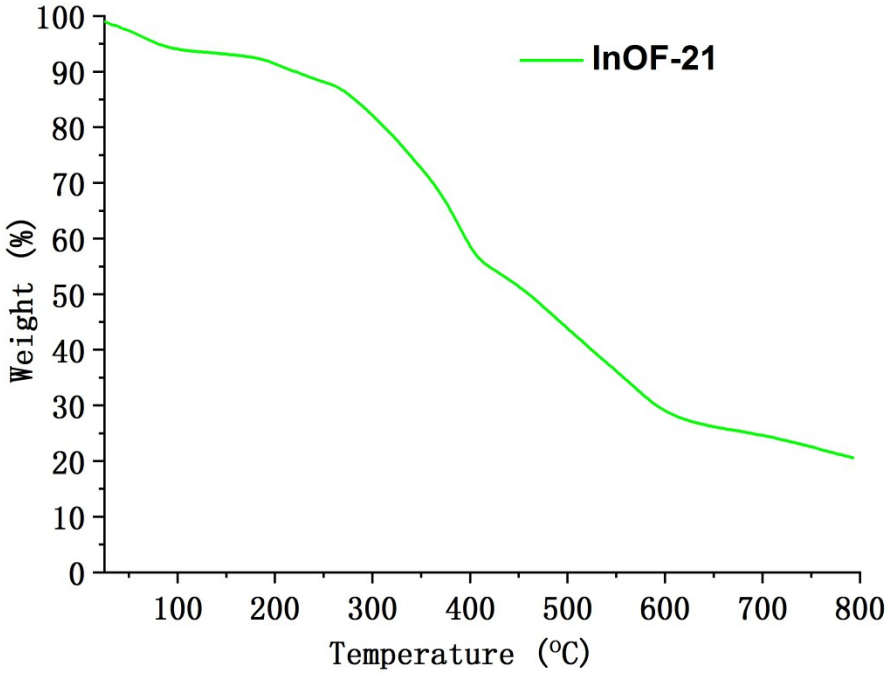

Figure S16. TGA curve for **InOF-21** samples.

Thermogravimetric analysis (TGA) measurements of **InOF-21** is conducted in the temperature range of 30-800 °C under a flow of nitrogen with the heating rate of 10°C min^{-1}.**InOF-21** shows a weight loss of ca.10.86% from 25-250 °C, which can be reasonably attributed to the loss of three guest H_2O molecules and one guest DEF molecule (calcd 10.35%), and then the main framework begins to quickly collapses upon further heating @ 350 °C (Figure S15).

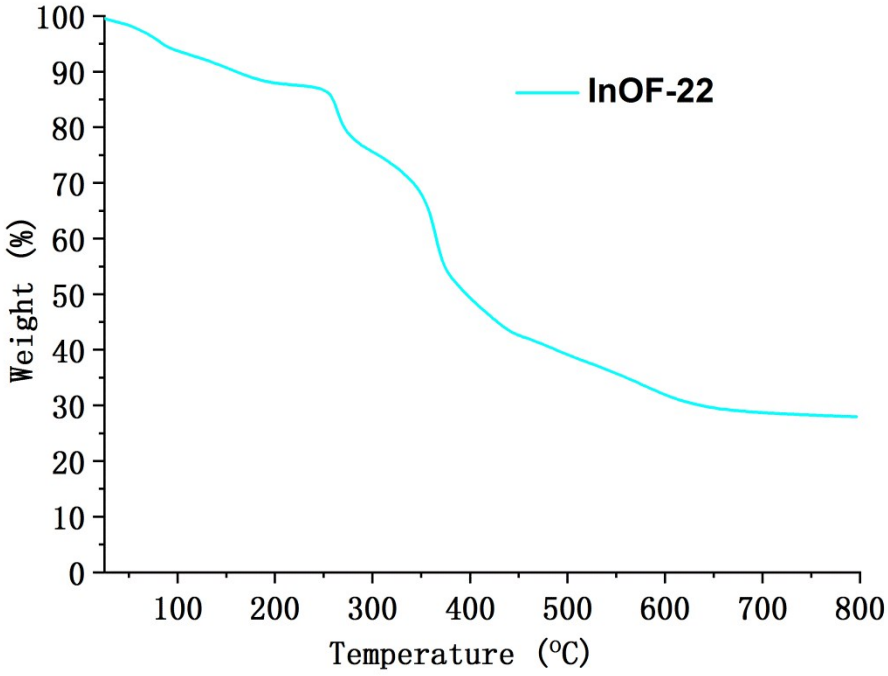

Figure S17. TGA curve for **InOF-22** samples.

Thermogravimetric analysis (TGA) measurements of **InOF-22** is conducted in the temperature range of 30-800 °C under a flow of nitrogen with the heating rate of 10°C min^{-1}.**InOF-22** shows a weight loss of ca.12.87% from 25-240 °C, which can be reasonably attributed to the loss of six guest H_2O molecules (calcd 12.70%), and then the main framework begins to quickly collapses upon further heating @350 °C (Figure S17).

S6. Sorption Analyses

N_2, CH_4, $H_2$and CO_2 Isotherms. All the N_2 and CO_2 isotherms for **InOF-19~22** were determined using an IGA gravimetric adsorption apparatus at the Fujian Institute of Research on the Structure of Matter in a clean ultra high vacuum system. Before measurements, about 100 mg solvent-exchanged samples were loaded into the sample basket within the adsorption instrument (ASAP 2020) and then degassed under dynamic vacuum at 100 ^{o}C for 10 h to obtain the fully desolvated samples[S5]. The N_2 sorption measurement was performed at 77 K, the CO_2 sorption measurement was performed at 293 K. The high-pressure H_2 excess adsorption isotherm at 77 K for **InOF-22** and the high-pressure CH_4 excess sorption isotherm at 273 K for **InOF-22**.

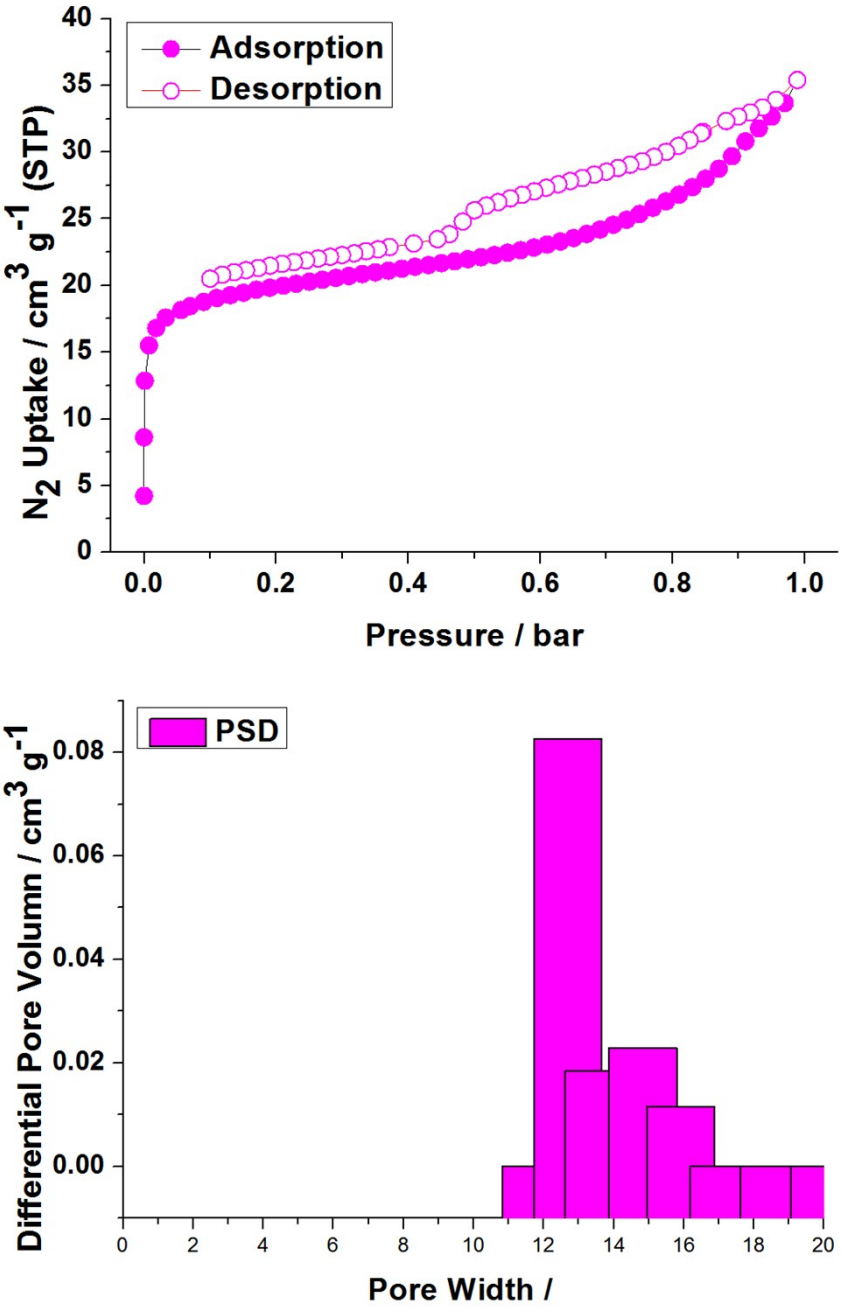

Figure S18. Experimental nitrogen sorption isotherms at 77 K for **InOF-20**; ● adsorption, ○ desorption. The bottom shows the pore size distribution (PSD) based on DFT calculation.

InOF-20 shows the quasi-reversible type-I N_2 isotherms with a relatively small hysteresis, which exhibits an inferior saturated uptake of 35.40 cm^3 g^{-1} and a major pore size distribution (PSD) at ~13 Å (Figure S18).In this case, we assume that at the higher temperature, these desolvated materials might undergo a critical state

leading to a distinct transition from microporosity to mesoporosity largely due to partial decomposition of the BTB(III) ligand and breakage of In-O coordination bonds.

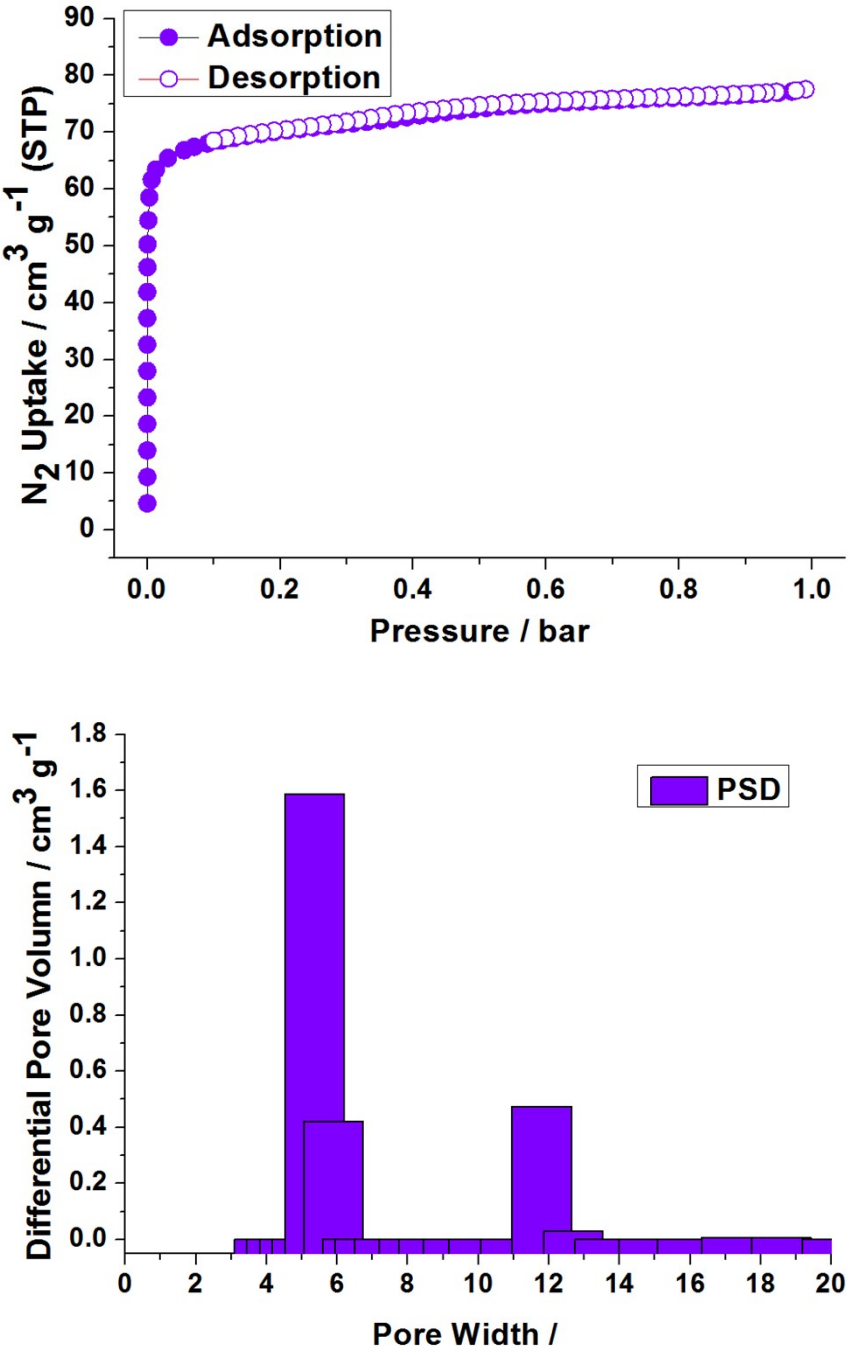

Figure S19. Experimental nitrogen sorption isotherms at 77 K for **InOF-21**; ● adsorption, ○ desorption. The bottom shows the pore size distribution (PSD) based on DFT calculation.

InOF-21 shows the quasi-reversible type-I N_2 isotherms with a relatively small hysteresis, which exhibits an inferior saturated uptake of 77.55 $cm^3\ g^{-1}$, and a major pore size distribution (PSD) at ~5 Å (Figure S18).

Table S3. Summary of the Porosity, BET SAs, Langmuir SAs, Pore volume and Pore size in **InOF-19~22**.

	InOF-19	**InOF-20**	**InOF-21**	**InOF-22**
Porosity	29.6%	17.6%	33.3%	66.2%
BET SAs($m^2 g^{-1}$)	124.2	75.0	275.7	1801.3
Langmuir SAs ($m^2 g^{-1}$)	157.1	132.7	334.2	1995.7
Pore volume(Calc.) ($Å^3$)	1059.4	1106.4	1211.4	7322.2
Pore volume(Expe.) ($cm^3 g^{-1}$)	0.063	0.054	0.118	0.707
Pore size (Å)	13	13	5	8

To investigate the CO_2, H_2 and CH_4 adsorption in **InOF-22**, the Grand canonical Monte Carlo (GCMC) simulations were carried out using the Sorption module of Materials Studio 8.0 package.[S6] The materials in the simulation were modeled as rigid structures, which ignores the skeleton stretching and bending vibration. The number of unit cells in the simulation box is 2×2×2 and periodic boundary conditions were applied in all directions. The Dreiding force field was used and the charges calculated via the Q_{eq} charge equilibration. In GCMC simulations, chemical potentials obtained by Peng-Robinson equation of state were taken as inputs to calculate the gas adsorption.

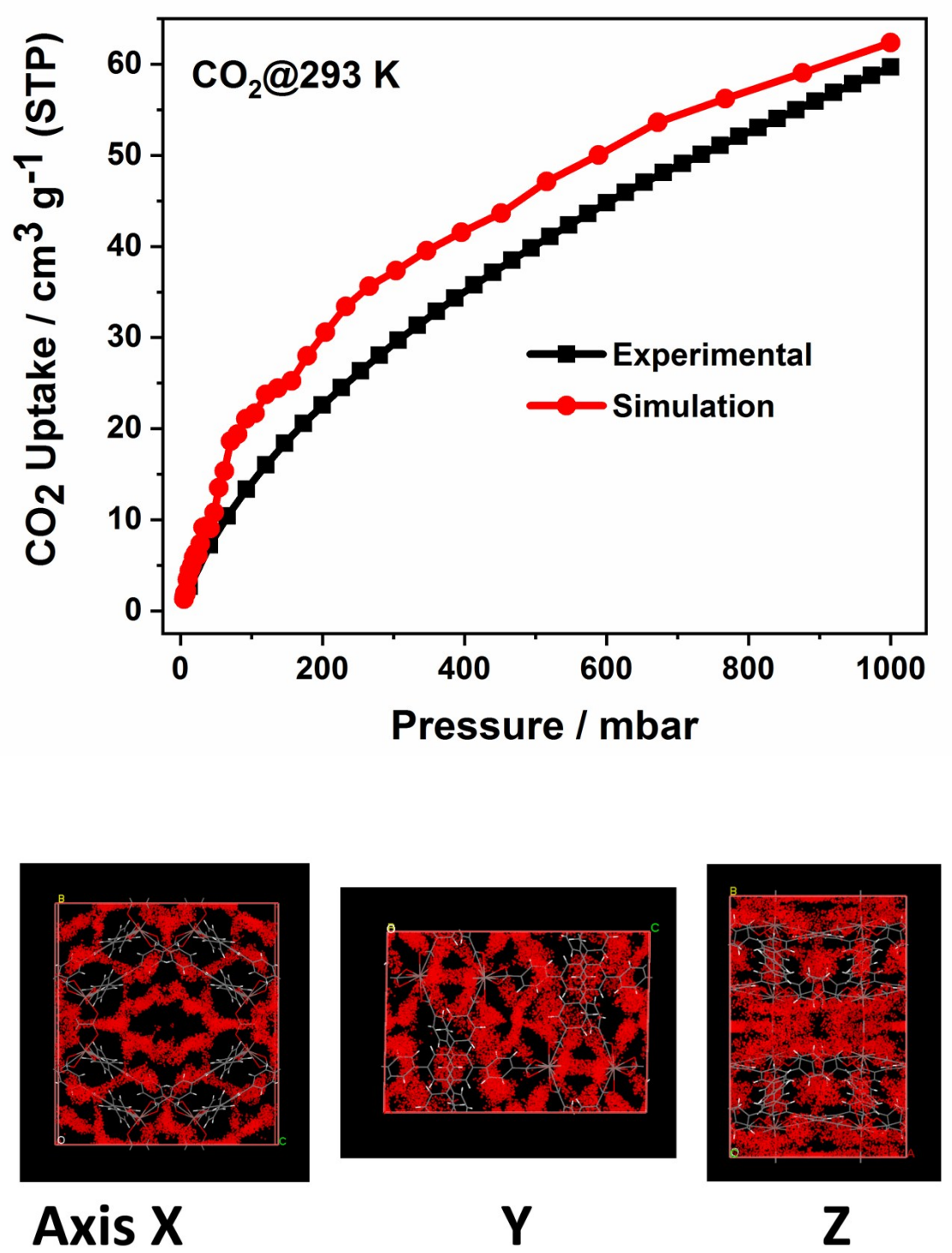

Figure S20. The simulated adsorption and experimental isotherm for CO_2 of **InOF-22**at 293 K and the CO_2 molecules' distribution probability in the 2*2*2 super cell.

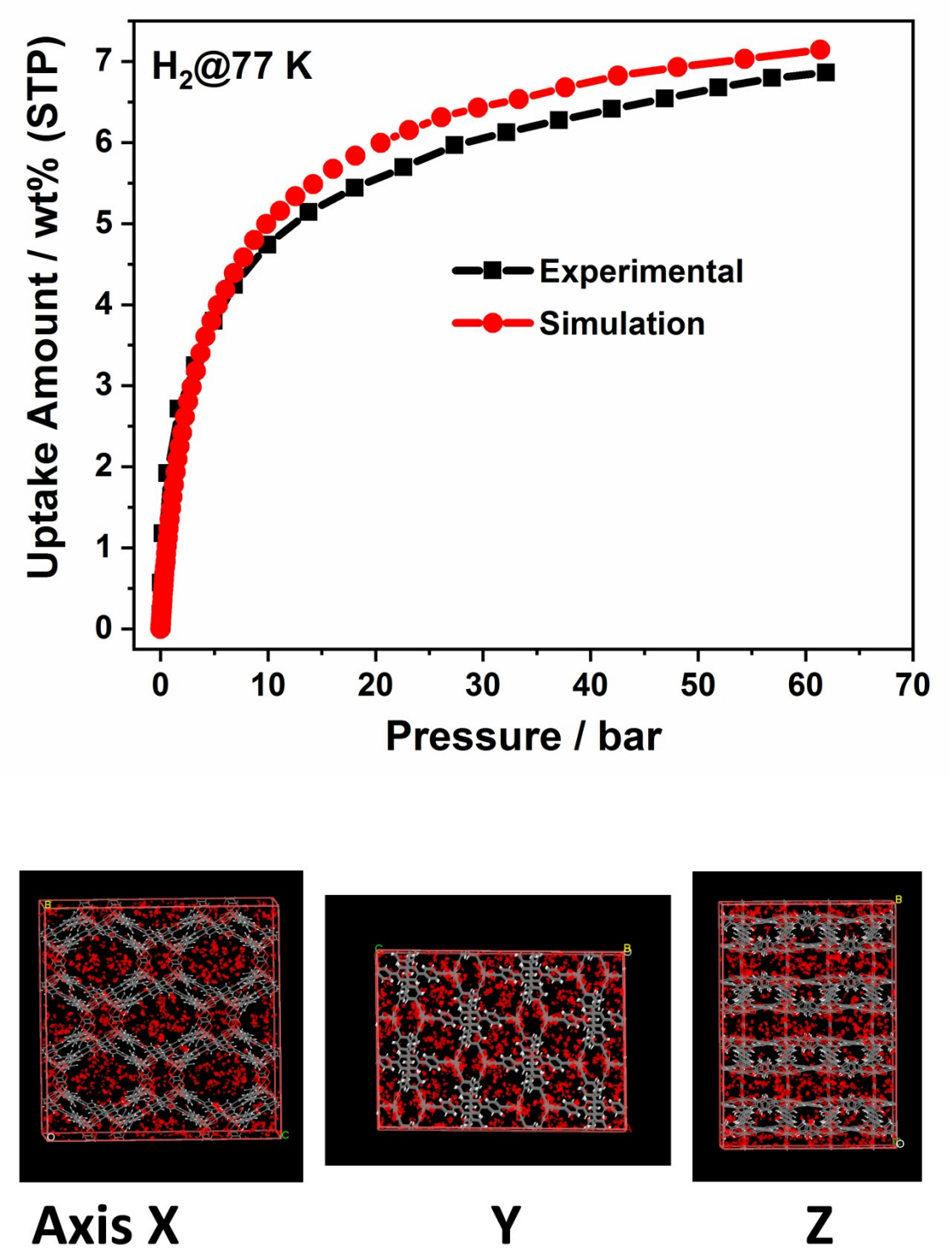

Figure S21. The simulated adsorption and experimental isotherm for H_2 of **InOF-22**at 77 K and the H_2 molecules' distribution probability in 2*2*2 the super cell.

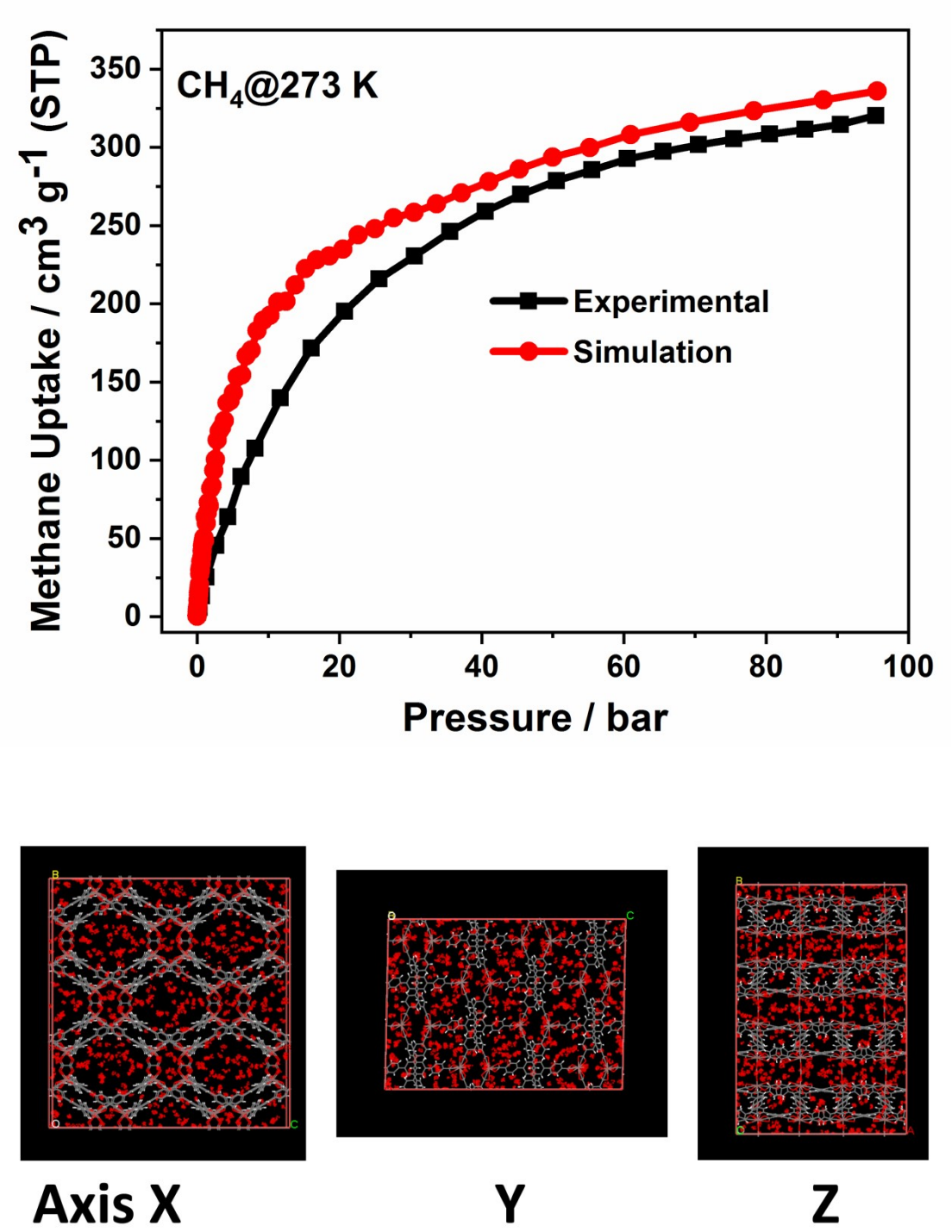

Figure S22. The simulated adsorption and experimental isotherm for CH_4 of **InOF-22** at 273 K and the CH_4 molecules' distribution probability in the 2*2*2 super cell.

Table S4. Comparison of Excess CO_2 uptake between **InOF-19~22** and well-known MOFs.

Compounds	CO_2 uptake at 1 atm ($cm^3\ g^{-1}$)	Ref
SIFSIX-2-Cu-i	121	S7
MPM-1-TIFSIX	90	S7
Bio-MOF-11	92	S7
FJI-H14	146	S7
UTSA-16	96	S7
Mmen-CuBTTri	94	S7
Cu-TDPAT	132	S7
HKUST-1	72	S7
PCN-88	94	S7
InOF-19	37.2	This work
InOF-20	30.5	This work
InOF-21	17.7	This work
InOF-22	62.4	This work
InOF-15	78	S8
InOF-17	54.24	S9
FJI-7	47.6	S10
ZIF-25	24	S11
ZIF-71	14.6	S11
ZIF-93	36.1	S11
ZIF-96	47.3	S11
ZIF-97	23.1	S11
IRMOF-3	25.1	S11
NH_2-MIL-53	35.8	S11

S7. References

[S1] O. V. Dolomanov, L. J. Bourhis, R. J. Gildea, J. A. K. Howard and H. Puschmann, *J. Appl. Cryst*. **2009**, *42*, 339.

[S2] SHELXS, G.M. Sheldrick, *Acta Cryst*. **2008**, A*64*, 112.

[S3] a) A. L. Spek, *J. Appl. Crystallogr.***2003**, *36*, 7; b) P. v.d. Sluis and A. L. Spek, *Acta Crystallogr., Sect. A*, **1990**, *46*, 194.

[S4] a) Q. R. Fang, G. S. Zhu, M. Xue, J. Y. Sun, F. X. Sun, S. L. Qiu, *Inorg. Chem.,***2006**, *45*, 3582; b) J. H. He, Y. T. Zhang, Q. H. Pan, J. H. Yu, H. Ding, R. R. Xu, *Micro. Meso. Mater.,***2006**, *90*, 145; c) S. Zheng, T. Wu, J. Zhang, M. Chow, R. A. Nieto, P. Feng, X. Bu, *Angew. Chem. Int. Ed.,***2010**, *49*, 5362; d) X. -R. Hao, X. -L. Wang, K. -Z. Shao, G. -S. Yang, Z. -M. Su, G. Yuan, *CrystEngComm.,* **2012**, *14*, 5596; (e) H. -L. Li, M. Eddaoudi, M. O'Keeffe, O. M. Yaghi, *Nature,* **1999**, *402*, 276.

[S5] ASAP 2020 Accelerated Surface Area and Porosimetry System Operator's Manual V4.00, Appendix C, C-43.

[S6] a) J. B. Hu, J. Liu, Y. Liu and X. Yang, *J. Phys. Chem. C.,***2016**, 120, 10311-10319; b) Y. Liu, H. L. Li and J. Liu, *Fuel.,***2016**, 184, 474-480; c) S. H. Yang, J. L. Sun, A. J. Ramirez-Cuesta, S. K. Callear, W. I. F. David, D. P. Anderson, R. Newby, A. J. Blake, J. E. Parker, C. C. Tang and M. Schröder, *Nat. Chem.,***2012**, 4, 887-894; d) Accelrys, Materials Studio Getting Started, release 8.0; Accelrys Software, Inc.: San Diego, CA, **2012**.

[S7] L. F. Liang, C. P. Liu, F. L. Jiang, Q. H. Chen, L. J. Zhang, H. Xue, H. L. Jiang, J. J. Qian, D. Q. Yuan and M. C. Hong, *Nat. Comm.,* **2017**, 8, 1233.

[S8] J. J. Qian, Q. P. Li, L. F. Liang, Ti. T. Li, Y. Hu and S. M. Huang, *Dalton Trans.,* **2017**, 46, 14102-14106.

[S9] Q. P. Li, Z. Y. Zhu and J. J. Qian, *Polyhedron.,* **2018**, 155, 218-222.

[S10] Q. P. Li, P. P. Yu, J. G. Luo and J. J. Qian, *Micro. and Meso. Mat.,* **2016**, 234, 196-199.

[S11] Q. J. Yan, Y. C. Lin, P. Y. Wu, L. Zhao, L. J. Cao, L. M. Peng, C. L. Kong and L. Chen, *ChemPlusChem.,* **2013**, 78, 86-91.